

Spatial Resolution Of A Noninvasive Measurement Of The Arterial And Venous Input Function Using A Wrist Monitor

Azael Villanueva, Jr., Sean P. Stoll, David J. Schlyer, Sepideh Shokouhi, Paul Vaska, Craig L. Woody, *Member, IEEE*, Aarti Kriplani, and Nora Volkow

Abstract--The current method for measuring the input function of a PET tomograph is by withdrawing arterial blood from a patient's wrist. In this study, the possibility of making a noninvasive measurement of the arterial blood is explored to determine the feasibility of using a planar set of detectors situated around the wrist. The arterial measurement was simulated using a peristaltic pump and an anatomically correct wrist phantom with attenuation. A step function was used to measure the activity flowing through arterial and venous tubing in the phantom. The detector was tested for spatial resolution and counting efficiency. The results showed the detector was able to discriminate the arterial and venous flows from noise when using planar coincidence images

I. INTRODUCTION

IN positron emission tomography (PET), a radiotracer is injected to measure the physiology of an organ or of other metabolic activities [1]. The radiotracer is first injected into the vascular system. Afterwards, it transfers from the vascular system into the cellular space thereby determining kinetics for its incorporation into a particular organ [2]. In order to extract the kinetic parameters, the blood radiotracer concentration needs to be measured as a function of time. This time activity curve is known as the input function. The current technique to measure the input function is through an invasive sampling of the blood [3]. The problems with this method are

the patient's discomfort and the medical personnel's risk in being exposed to potential blood borne diseases or radioactive contamination while collecting blood samples. Therefore, alternative noninvasive sampling devices are being considered to help determine the input function. This noninvasive approach would then minimize the patient and physician risks and simplify the gathering of kinetic information from a PET scan.

There are several techniques currently used in making a noninvasive measurement of the input function. These techniques include external monitors and PET scanners that measure standardized input functions, non-invasively sampled input functions or image derived input functions. The standardized input functions use a population based input function that gets correlated to an individual's physiological measurements [4]-[8]. However, the problem with this method was the physiological variability of an individual. The non-invasively sampled input functions used external monitors that measure the input function from an area outside a region of the body such as the neck, chest or wrist [9]-[11]. However, this method was not sensitive enough to differentiate the arterial input function from the background radiation noise. Therefore, more sensitive scanners such as PET tomographs or flat bed detector arrays were used to produce image derived input functions (IDIF). PET tomographs have been extensively used to monitor the IDIF from the heart [12]-[14], but these measurements require the use of two separate scanners to measure the kinetic parameters of the brain. Others have used the PET tomograph on the neck or brain to measure the IDIF [15]-[17]. Yet, with these scanners, they lacked the proper resolution of the radiation source since the scanning area is large as compared to the area within a blood vessel. Therefore, smaller scanners placed around the wrist could potentially have the best resolution at a more economical cost to measure the IDIF at high enough sensitivity.

Since the input function is often sampled from the radial artery, a new noninvasive detector (often referred to as the Arterial Wrist Monitor) is being designed to sample the radial arterial blood of the wrist (Fig. 1). Previously, some studies have tried measuring the input function from the wrist, but those monitors were not sensitive enough to produce the IDIF appropriately [18]-[20]. The approach taken here was to use a flat bed detector array made from lutetium oxyorthosilicate

Manuscript received May 9, 2003. This work was supported in part by a grant from the DOE Office of Biological and Environmental Research and DOE Contract DE-AC02-98CH10886U.S.

A. Villanueva is with SUNY @ Stony Brook, Stony Brook, NY USA (telephone: 631-344-4576, e-mail: azvilla@bnl.gov).

S. P. Stoll is with Brookhaven National Laboratory, Upton, New York 11973 (telephone: 631-344-5331, e-mail: stoll@bnl.gov).

D. J. Schlyer is with Brookhaven National Laboratory, Upton, New York 11973 (telephone: 631-344-4587, e-mail: schlyer@bnl.gov)

S. Shokouhi is with SUNY @ Stony Brook, Stony Brook, NY USA (telephone: 631-344-4576, e-mail: sepideh@bnl.gov).

P. Vaska is with Brookhaven National Laboratory, Upton, New York 11973 (telephone: 631-344-6228, e-mail: vaska@bnl.gov)

C. L. Woody is with Brookhaven National Laboratory, Upton, New York 11973 (telephone: 631-344-2752, e-mail: woody@bnl.gov)

A. Kriplani is with SUNY @ Stony Brook, Stony Brook, NY USA (telephone: 631-344-4576, e-mail: aarti@bnl.gov).

N. Volkow is with the National Institutes of Health, Bethesda, MD USA, on leave from Brookhaven National Laboratory, Upton, New York 11973 (e-mail: volkow@bnl.gov).

(LSO) in an array of 4x8 crystals. This detector would create planar images in a similar fashion to that of an Anger camera. It would also have better light collection crystals (made of LSO) than the one previously used [19] along with a small APD array that better matches the size and pixels of the crystal block. This technical advancement further reduces the size of the radial monitor while at the same time improving the statistics of the gamma detection. Each crystal in the array has the dimensions of 2x2x10 mm. The crystal array is attached directly to an avalanche photodiode (APD) for the conversion of scintillation photons to electronic signals [21]. Pairs of these arrays will be used to count the photons in coincidence over the radial artery of a wrist.

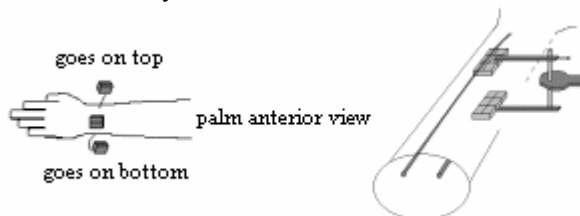


Fig. 1. The flat bed detector pair would be placed above and below the wrist. More than one pair may be used to differentiate the radial artery from venous and tissue background.

These coincidence counts can then be used to quantify the activity and produce an input function of the radiotracer concentration. To test how effective this new device would be in measuring the input function, the signal sensitivity and image resolution were measured using an anatomically correct wrist phantom. The wrist phantom simulates geometry of a human wrist and the attenuation associated with the location of the vessels. The phantom was also used to determine whether the wrist monitor could resolve the arteries and veins from each other. These results will then determine the performance level of this detector as it reaches completion of a model that can be used in a real clinical setting.

II. METHODOLOGY

A. Materials



Fig. 2. A wrist phantom of the left arm was used for these studies.

A wrist phantom with anatomically correct placement of blood vessels was designed using MRI images of the human wrist. The wrist phantom is composed of a Lucite block with two 4 mm diameter drilled internal holes representing the arteries and two 4 mm above-artery holes representing the

veins (Fig. 2). This phantom was to be mounted between the two detector arrays. It was then used to determine the amount of signal that could be obtained from both the artery and vein and the possible background noise (or interference) expected from a vein.

B. Experimental Method

In these experiments, a step function of a $^{11}\text{CO}_3^-$ or $^{18}\text{F}^-$ solution was used as a flow pulse. After priming the tubing with water, the solution (labeled “hot”) was switched in and pumped through the arterial holes (Fig. 3).

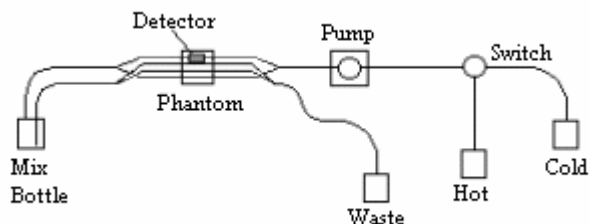


Fig. 3. The arterial line passes below and off the side of the venous line. The same detector pair would then measure both the arterial and venous concentrations.

The solution then flowed into a mixing bottle simulating the palm and afterwards flowed back through the venous holes. Thus, both the arterial and venous step functions were measured and analyzed for their image resolution. Two flow pulses were measured in this experiment. First, the solution containing the radioactivity was switched on for 1 minute and next switched off. After flushing the lines, this procedure was repeated with a two minute pulse of radioactivity. The tubing was designed to be long enough to pass one minute of the solution before the venous return starts to be detected.

In a different experiment, a sensitivity measurement was performed. This experiment had a flow pulse pumped in without the mixing bottle and venous return line. First, the wrist phantom was removed leaving the tubing at the same location it would be in the phantom. Then, another flow pulse was pumped in with the phantom mounted between the detectors. Thus, two step pulses were measured one with and the other without the attenuation of the phantom.

III. DATA PROCESSING AND ANALYSIS

For the creation of a planar image with minimal Compton scattered events, counts were analyzed using only coincidence events between a crystal element and the element in the other crystal array exactly opposite. This type of image produced an image with high resolution. Also, to recreate planar images with shorter time intervals, focal plane imaging was implemented as a means to use all the counts occurring between the detectors and above two thresholds that discriminate noise and low energy Compton events. First, the 511 keV photopeaks were identified through the use of histograms of the pulse height spectra. Next, using all of the counts detected above a hardware threshold of 200 keV, the time activity curve was analyzed and decay corrected to determine the time points of the step function pulses and the

efficiency of the wrist monitor. Lastly, planar images were made for selected periods of time using a software threshold of 400 keV (photoelectron energies above 80% of the photopeak), which further minimized Compton scattered events. All these computations were done in C++.

IV. RESULTS

A. Sensitivity effects

To determine how close the detector sensitivity was to a theoretical value, the geometrical effects and detector system efficiencies were evaluated. The wrist phantom has dimensions of 5 cm in thickness with the arterial hole lying in between 3.2 cm from the left detector and 1.8 cm from the right and the venous hole lying in between 4.6 cm from the left detector and 0.4 cm from the right. Using these wrist phantom dimensions, it can be shown that the two detectors have an azimuthal angle efficiency of 8% and an axial efficiency of 36%. From previous calculations, the system efficiency still contains a 60% stopping power within a 10 mm crystal and an electronic discrimination of 40% resulting in a measured system efficiency of 24% [21]. Therefore, the combined theoretical detector sensitivity was calculated to be: $37 \text{ dps/nCi} * (0.08 * 0.36 * 0.24^2) \text{ cps/dps} = 0.061 \text{ cps/nCi}$.

C-11 Attenuation effects 6/04/03

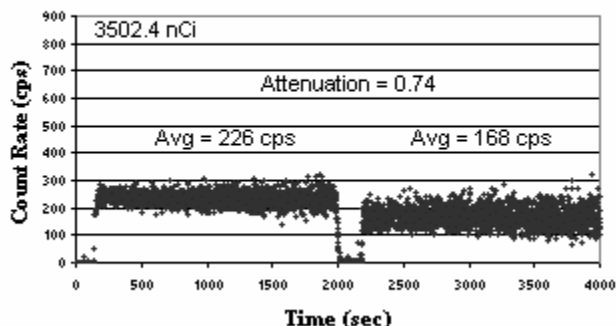


Fig. 4. Sensitivity measurement of the wrist monitor. The first pulse is a measurement without the wrist phantom. The second pulse has the wrist phantom mounted back between the detectors.

As for the sensitivity measurement, Fig. 4 shows the attenuation of the lucite wrist phantom comparing an unattenuated signal to an attenuated signal. The measured sensitivity seen by this detector’s field of view of 0.05 cm^3 was $226 \text{ cps} / 3500 \text{ nCi} = 0.064 \text{ cps/nCi}$, which is in good agreement with the theoretical value. This value, however, does not include the wrist phantom attenuation factor, which has a value of 0.74 ($168 \text{ cps} / 226 \text{ cps}$).

B. Venous return time activity curves

In the venous return measurement, the one minute pulse showed clearance of the arterial activity before the venous activity started to be detected in the venous return line (Fig. 5). This figure clearly shows two separate input functions, the

arterial and the venous, which the wrist monitor could differentiate if there was enough time delay between them.

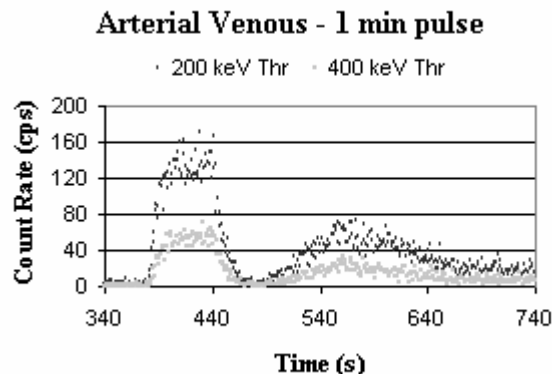


Fig. 5. One minute pulse clearance of arterial activity.

However, in a real patient’s wrist measurement, these two input functions overlap within seconds. Therefore, the two minute pulse was setup to have an overlap between the arterial and venous activity to see if the wrist monitor would have enough resolution to differentiate the arterial activity from the venous interference (Fig. 6).

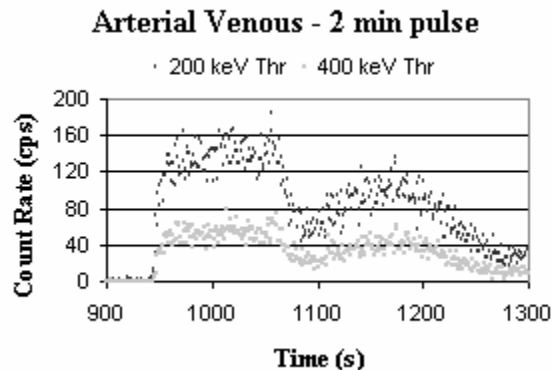


Fig. 6. Two minute pulse overlap of artery and vein.

For both pulses at the 200 keV threshold setting, the total coincident counts detected with the wrist phantom in place was measured to be 137.5 ± 14.4 counts at every 1-sec interval, which includes random and Compton scattered events. Reducing most of the scattered events with a 400 keV threshold gives an average rate of 53.6 ± 7.2 cps. This would be the maximum count rate both the high resolution image and focal plane image can have using the 400 keV threshold. As for this measurement’s sensitivity, the total activity used in this experiment was 3950 nCi, which is decay corrected to the start of the data acquisition. Using the total activity and the measured rate of 137.5 cps, the sensitivity of this measurement came to be 0.035 cps/nCi. Dividing by the theoretical sensitivity, the attenuation in this case came to be 0.57. This lower number may be a result of the variability in the detection of attenuated events.

C. High resolution planar imaging

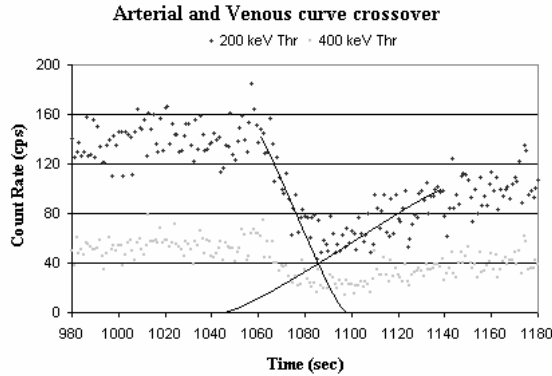


Fig. 7. Overlap of the arterial step pulse and the venous step pulse for both the hardware 200 keV threshold and the software 400 keV threshold. The high resolution planar image will sort through all the counts in the span of 100 sec (1030-1130 sec). The lines demarcate a probable end and beginning of the arterial and venous step pulses, respectively.

The high resolution planar image was made using the overlap activity of the 2 minute pulse, which occurred between 1030-1130 sec (Fig. 7). The arterial and venous lines could be resolved at a separation of 4 mm between the center of both columns (Fig. 8).

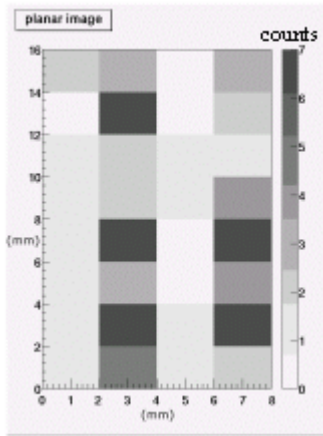


Fig. 8. Planar image of the artery on the left and the vein on the right. This figure shows that we are clearly able to visualize the artery and vein independently. The scale to the left is a measure of the number of coincident counts in each pixel.

The actual separation of both holes on the left of the wrist phantom in Fig. 2 is 2 mm, which is 1 mm + 1 mm of the tubing outer shell when having an outer diameter of 4 mm and inner diameter of 2 mm. Therefore, this measurement lies in good agreement with the placement of the activity source.

The sensitivity of this image was 78 counts for 100 sec. The rate was not high enough in this mode (high resolution, planar coincidence) to garner enough counts for producing an IDIF. Therefore, counts at other angles were included to increase the sensitivity within a shorter time interval. The focal plane imaging method was employed to use these other counts and provide better sensitivity, but at a cost of including more scattered events.

D. Focal Plane Imaging

Dynamic images were generated at 10 sec intervals of the 200 sec overlap time span seen in Fig. 7. First, the arterial plane at a depth of 1.8 cm was imaged for a total of 20 frames (Fig. 9(a)). Next, the venous plane at a depth of 0.4 cm was imaged for another 20 frames (Fig. 9(b)). The 10 middle frames, 6-15, are used here to show the overlap of the two activity curves.

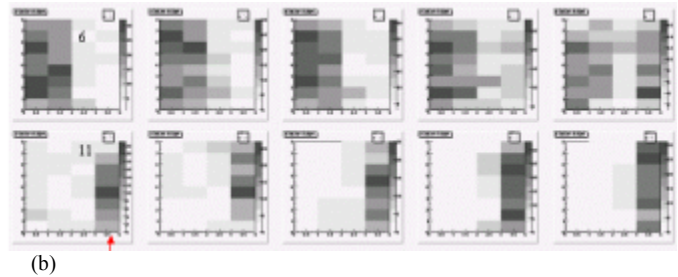
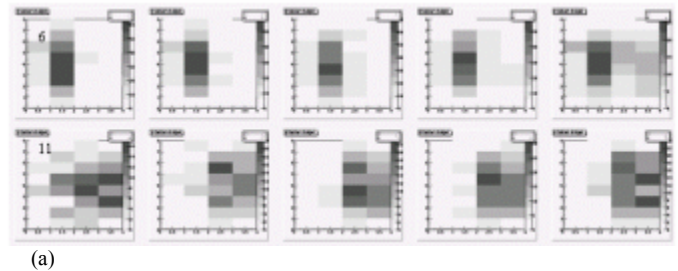


Fig. 9. (a) These are frames 6-15 of the arterial focal depth of 1.8 cm. (b) These are frames 6-15 of the venous focal depth of 0.4 cm. Note how the arterial line blurs out on the second column of frame 11 and the venous line blurs in on the fourth column of frame 10.

Image derived step function plus venous return

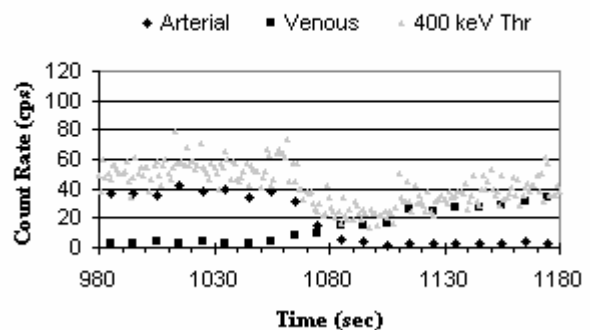


Fig. 10. Image derived step function for both the arterial and venous step pulses. Note that only the 400-keV threshold is used here since it is the maximum number of counts possible after the software discrimination for scatter.

Using these time frames, the total number of counts was summed per each column (column 2 for arterial as seen in Fig. 9a and column 4 for venous as seen in Fig. 9b). These summed totals were then plotted as image-derived step functions (Fig. 10). The step pulse for both the arterial and venous activity agreed well with the activity at the 400 keV

threshold. The max count rate went from 137.5 cps (400keV, Fig. 7) to 53.6 cps (200 keV, Fig. 10) to 37.9 cps (arterial IDIF, Fig. 10). The first loss in count rate is due to Compton scatter discrimination and the second loss is probably due to the image resolution detection.

V. DISCUSSION AND CONCLUSION

The attenuation of the wrist medium and the distance between the detectors played a critical role in the detector's sensitivity and signal to noise ratio. The typical maximum blood activity in a PET study is around 2.5 $\mu\text{Ci/cc}$. Although the activity used here may have been too high, we were able to provide with one detector pair a good resolution of the arterial and venous lines using counts above a software threshold of 400-keV. It seems feasible that this technology could be used to measure the input function at more appropriate blood activity levels, provided the sensitivity can be increased. To increase the sensitivity, we can use more detector blocks and arrange them along the artery so that they could acquire more coincident counts and produce less noisy time activity curves. We can also increase crystal length and perform energy corrections for any cross talk occurring between crystals [22]. To improve and optimize the image quality, we can perform corrections of the focal plane images through normalization measurements and scatter background estimations. Other future design considerations may be external background checks for determining the amount of wrist monitor shielding and tissue background measurements for a quantitative determination of low levels of activity (~ 200 nCi/cc).

VI. ACKNOWLEDGMENT

The authors sincerely acknowledge Proteus and CTI, Inc. This work is part of a joint collaboration between Brookhaven National Lab, and Stony Brook University.

VII. REFERENCES

- [1] M. E. Phelps, J. Mazziotta, and H. Schelbert, *Positron Emission Tomography and Autoradiography: Principles and Applications for the Brain and Heart* Raven Press, New York, 1986, pp. 287-346.
- [2] T. F. Budinger and R. H. Huesman, "Ten precepts for quantitative data acquisition and analysis," *Circulation*, vol. 72, no. 5 Pt 2, pp. 53-62, Nov. 1985.
- [3] J. R. Votaw and S. D. Shulman, "Performance evaluation of the picocount flow-through detector for use in cerebral blood flow PET studies," *J. Nucl. Med.*, vol. 39, pp. 509-515, 1998.
- [4] S. Takikawa, V. Dhawan, P. Spetsieris, W. Robeson, T. Chaly, R. Dahl, D. Margouff, and D. Eidelberg, "Noninvasive quantitative fluorodeoxyglucose PET studies with an estimated input function derived from a population-based arterial blood curve," *Radiology*, vol. 188, pp. 131-136, 1993.
- [5] N. Sadato, Y. Yonekura, M. Senda, Y. Magata, Y. Iwasaki, N. Matoba, T. Tsuchida, N. Tamaki, H. Fukuyama, H. Shibasaki, and J. Konishi, "Noninvasive measurement of regional cerebral blood flow change with H_2^{15}O and positron emission tomography using a mechanical injector and a standard arterial input function," *IEEE Trans. Med. Imaging*, vol. 12, pp. 703-710, 1993.
- [6] S. Eberl, A. R. Anayat, R. R. Fulton, P. K. Hooper, and M. J. Fulham, "Evaluation of two population-based input functions for quantitative neurological FDG PET studies," *Eur. J. Nucl. Med.*, vol. 24, pp. 299-304, 1997.
- [7] T. Tsuchida, N. Sadato, Y. Yonekura, S. Nakamura, N. Takahashi, K. Sugimoto, A. Waki, K. Yamamoto, H. Nobushige, and Y. Ishii, "Noninvasive measurement of cerebral metabolic rate of glucose using standardized input function," *J. Nucl. Med.*, vol. 40, pp. 1441-1445, 1999.
- [8] T. Shiozaki, N. Sadato, M. Senda, K. Ishii, T. Tsuchida, Y. Yonejura, H. Fukuda, and J. Konishi, "Noninvasive estimation of FDG input function for quantification of cerebral metabolic rate of glucose: Optimization and multicenter evaluation," *J. Nucl. Med.*, vol. 41, pp. 1612-1618, 2000.
- [9] J. E. Litton and L. Eriksson, "Transcutaneous measurement of the arterial input function in positron emission tomography," *IEEE Trans. Nucl. Sci.*, vol. 37, pp. 627-628, 1990.
- [10] A. D. Nelson, F. Miraldi, R. F. Muzic, G. P. Leisure, and W. E. Semple, "Noninvasive arterial monitor for quantitative oxygen-15-water blood flow studies," *J. Nucl. Med.*, vol. 34, pp. 1000-1006, 1993.
- [11] H. Watabe, M. Miyake, Y. Narita, T. Nakamura, and M. Itoh, "Development of skin surface radiation detector system to monitor radioactivity in arterial blood along with positron emission tomography," *IEEE Trans. Nucl. Sci.*, vol. 42, pp. 1455-1459, 1995.
- [12] K. Yoshida, M. Endo, H. Fukuda, A. Kagaya, T. Himi, Y. Masuda, Y. Inagaki, T. Iinuma, T. Yamasaki, and Y. Tateno, "Measurement of arterial tracer concentrations from cardiac PET images," *J. Comput. Assist. Tomogr.*, vol. 19, pp. 182-187, 1995.
- [13] H. Iida, S. Miura, Y. Shoji, T. Ogawa, H. Kado, Y. Narita, J. Hatazawa, S. Eberl, I. Kanno, and K. Uemura, "Noninvasive quantitation of cerebral blood flow using oxygen-15-water and a dual-PET system," *J. Nucl. Med.*, vol. 39, pp. 1789-1798, 1998.
- [14] A. P. van der Weerd, L. J. Klein, R. Boellaard, C. A. Visser, F. C. Visser, and A. A. Lammertsma, "Image-derived input functions for determination of MRGlu in cardiac 18F-FDG PET scans," *J. Nucl. Med.*, vol. 42, pp. 1622-1629, 2001.
- [15] F. Iannotti, C. Fieschi, B. Alfano, P. Picozzi, L. Mansi, C. Pozzilli, A. Punzo, G. Del Vecchio, G. L. Lenzi, M. Salvatore, and P. Conforti, "Simplified, noninvasive PET measurement of blood-brain barrier permeability," *J. Comp. Assist. Tomogr.*, vol. 11, pp. 390-397, 1987.
- [16] D. Feng, K. P. Wong, C. M. Wu, and W. C. Siu, "A technique for extracting physiological parameters and the required input function simultaneously from PET image measurements: Theory and simulation study," *IEEE Trans. Inf. Technol. Biomed.*, vol. 1, pp. 243-254, 1997.
- [17] K. Chen, D. Band, E. Reiman, S. C. Huang, M. Lawson, D. Feng, Y. Lang-sheng, and P. Anita, "Noninvasive quantification of the cerebral metabolic rate for glucose using positron emission tomography, ^{18}F -fluoro-2-deoxyglucose, the Patlak method, and an image-derived input function," *J. Cereb. Blood Flow Metab.*, vol. 18, pp. 716-723, 1998.
- [18] L. Eriksson and I. Kanno, "Blood sampling devices and measurement" *Medical Progress through Technology*, vol. 17, pp. 249-257, 1991.
- [19] S. Rajeswaran, D. L. Bailey, S. P. Hume, D. W. Townsend, A. Geissbuhler, J. Young, and T. Jones, "2-D and 3-D imaging of small animals and the human radial artery with a high resolution detector for PET," *IEEE Trans. Med. Imaging*, vol. 11, pp. 386-391, 1992.
- [20] M. Aykac, R. D. Hichwa, and G. L. Watkins, "Investigation of a noninvasive detector system for quantitative [O-15] water blood flow studies in PET," *IEEE Trans. Nucl. Sci.*, vol. 48, pp. 31-37, 2001.
- [21] S. Shokouhi, S. P. Stoll, A. Villanueva, P. Vaska, D. J. Schlyer, C. L. Woody, B. Yu, P. O'Conner, J. F. Pratte, V. Radeka, N. Volkow, and J. S. Fowler, "A non-invasive LSO-APD blood radioactivity monitor for PET imaging studies," *IEEE Trans. Nucl. Sci.*, 2003 (in press).
- [22] P. Vaska, S. P. Stoll, C. L. Woody, D. J. Schlyer, and S. Shokouhi, "Effects of inter-crystal cross-talk on multi-element LSO/APD PET detectors," *IEEE Trans. Nucl. Sci.*, 2003 (in press).